© 2018. This manuscript version is made available under the CC BY-NC-ND 4.0 license
http://creativecommons.org/licenses/by-nc-nd/4.0/

*Article*

# Assessment of atmospheric correction methods for Sentinel-2 images in Mediterranean landscapes

**Ion Sola [1]*, Alberto García-Martín[2,3], Leire Sandonis-Pozo [4], Jesús Álvarez-Mozos [1], Fernando Pérez-Cabello [3,4] María González-Audícana [1] and Raquel Montorio Llovería [3,4]**

[1] Universidad Pública de Navarra. Departamento de Proyectos e Ingeniería Rural, c/Campus Arrosadía s/n 31006 Pamplona.
[2] Centro Universitario de la Defensa de Zaragoza, Academia General Militar. Ctra. Huesca s/n, 50090 Zaragoza, Spain; algarcia@unizar.es
[3] GEOFOREST research group, Environmental Sciences Institute (IUCA), University of Zaragoza, C/ Pedro Cerbuna 12, 50009 Zaragoza, Spain.
[4] Department of Geography and Spatial Management, University of Zaragoza, C/ Pedro Cerbuna 12, 50009 Zaragoza, Spain; l.sandonisp@gmail.com; fcabello@unizar.es; montorio@unizar.es
* Correspondence: ion.sola@unavarra.es; Tel.:948168401

Academic Editor: name
Received: date; Accepted: date; Published: date

**Abstract:** Atmospheric correction of optical satellite imagery is an essential pre-processing for modelling biophysical variables, multi-temporal analysis, and digital classification processes. Sentinel-2 products available for users are distributed by the European Space Agency (ESA) as Top Of Atmosphere reflectance values in cartographic geometry (Level-1C product). In order to obtain Bottom Of Atmosphere reflectance images (Level-2A product) derived from this Level-1C products, ESA provides the SEN2COR module, which is implemented in the Sentinel Application Platform. Alternatively, ESA recently distributes Level-2A products processed by SEN2COR with a default configuration. On the other hand, the conversion from Level-1C to Level-2A product can be generated using alternative atmospheric correction methods, such as MAJA, 6S, or iCOR. In this context, this paper aims to evaluate the quality of Level-2A products obtained through different methods in Mediterranean shrub and grasslands by comparing data obtained from Sentinel-2 imagery with field spectrometry data. For that purpose, six plots with different land covers (asphalt, grass, shrub, pasture, and bare soil) were analyzed, by using

synchronous imagery to fieldwork (from July to September 2016). The results suggest the suitability of the applied atmospheric corrections, with coefficients of determination higher than 0.90 and root mean square error lower than 0.04 achieving a relative error in bottom of atmosphere reflectance of only 2-3%. Nevertheless, minor differences were observed between the four tested methods, with slightly varying results depending on the spectral band and land cover.

**Keywords:** Sentinel 2A-MSI; Atmospheric correction; SEN2COR; MAJA; 6S; iCOR; Field spectrometry; Mediterranean shrub and grasslands

## 1. Introduction

The pair of Sentinel-2 (S2) satellites provides improved continuity for Spot- and Landsat-type observations due to their complete interoperability with these programs (Drusch et al., 2012), increasing the quantity of available images to use in several applications where medium-high resolution optical images have been shown useful. In addition, S2 presents some advantages over Landsat and SPOT space programs (Astrium, 2013; Gascon et al., 2017; Zanter, 2015): (i) a higher spectral resolution in the optical spectrum than Landsat 8 (L8) and SPOT 5; (ii) a greater spatial resolution along the entire optical spectrum, compared to L8; (iii) a more extensive swath (around 280 $km^2$ compared to the 185 $km^2$ of Landsat and the 60 $km^2$ of SPOT 5) and; (iv) a higher temporal resolution than L8 (Sentinel-2A and Sentinel-2B together will provide a global median average revisit interval of 5 days overtaking significantly the 16 days of Landsat).

In the short period of time since Sentinel-2A, and more recently Sentinel-2B, became fully operative, many studies have been performed testing the application of these observations to land cover classification (Borràs et al., 2017; Shoko and Mutanga, 2017), crop mapping (Immitzer et al., 2016; Lebourgeois et al., 2017), biophysical parameter estimation (Clevers et al., 2017; Chrysafis et al., 2017; Sibanda et al., 2016; Vuolo et al., 2016), forest fires (Navarro et al., 2017; Quintano et al., 2016; Verhegghen et al., 2016), water resources (Dörnhöfer et al., 2016; Toming et al., 2016;

Traganos and Reinartz, 2017) or urban areas characterization (Lefebvre et al., 2016; Pesaresi et al., 2016; Yang and Chen, 2017). In addition, there is also an increasing amount of scientific literature combining or comparing S2 with L8 images (Colkesen and Kavzoglu, 2017; Korhonen et al., 2017; Mallinis et al., 2017; Munyati, 2017; Novelli et al., 2016; Paul et al., 2016; van der Meer et al., 2014).

Since 2015, the European Space Agency (ESA) provides Level-1C products derived from Sentinel-2A and from 29 June 2017 also for Sentinel-2B. Level-1C data corresponds to Top-Of-Atmosphere (TOA) reflectance values after the application of radiometric and geometric corrections (including orthorectification and spatial registration). Besides, the Copernicus Open Access Hub provides Level-2A products of S2 imagery data over Europe (EEA-39) from 28 March 2017. Level-2A corresponds to Bottom-Of-Atmosphere reflectances (BOA). The production of S2 Level-2A products is done using SEN2COR processor (version 2.3.1) (ESA, 2015; Gascon et al., 2017; Louis et al., 2016). This processor developed by ESA performs the atmospheric correction (AC), terrain and cirrus correction and scene classification applied to the mentioned TOA Level-1C input data. For this production the PlanetDEM Digital Elevation Model (DEM) is used, while cirrus and Bidirectional Reflectance Distribution Function (BRDF) corrections are deactivated.

ESA also distributes SEN2COR processor freely, as a plugin integrated in the Sentinel Application Platform software (SNAP). Besides of the BOA reflectance product, additional outputs such as Aerosol Optical Thickness (AOT) map, Water Vapor (WV) map, Scene Classification map and Quality Indicators data are generated. The atmospheric model of SEN2COR is based on the ATCOR model, which inverts the parameters previously mentioned through the use of transformation tables (LUT's, *Look Up Table*), obtained from Radiative Transfer Models (RTM) calculated over the type of sensor, solar geometry, topography of the terrain and atmospheric parameters. Further details on SEN2COR processor and its calibration can be obtained in (Müller-Wilm, 2016; Richter et al., 2017).

The accuracy of the AC applied to an optical image is a very relevant factor because it essentially affects the accuracy of: (i) multi-temporal studies; (ii) the inter-comparison of

measurements from different optical sensors; (iii) the improvement of digital classification processes; and (iv) the development of physical and empirical models to estimate biophysical variables (e.g.: Leaf Area Index, LAI; Fraction of Absorbed Photosynthetically Active Radiation by the green elements of the canopy, FAPAR; Canopy water content, CWC; Above Ground Biomass, AGB) (Chuvieco, 2010; Gascon et al., 2017; Lillesand et al., 2014; Marcello et al., 2016; Pons et al., 2014; Vuolo et al., 2016).

In particular, the performance of AC relies on an accurate estimation of the concentration and type of atmospheric particles at the acquisition time (Vermote and Kotchenova, 2008). The aerosol contribution still generates high uncertainties in the correction of atmospheric effects though (Vermote et al., 1997). In the last years, research institutes, aerospace agencies and private companies have developed AC methods for high spatial resolution (HSR) multispectral images (Hagolle et al., 2015a; Lantzanakis et al., 2017; Martins et al., 2017; Nazeer et al., 2014). Some of these methods have been successfully applied, and at present the selection of the best AC method to be applied to S2 Level-1C products is a hot topic under discussion, as demonstrated by the Atmospheric Correction Inter-comparison Exercise (ACIX), an international collaborative initiative to inter-compare a set of AC methods for HSR optical sensors, specially focused on L8 and S2 imagery (Doxani et al., 2018).

The accuracy of the S2 Level-2A products obtained through different AC processors must be validated. In the case of SEN2COR, the Level-2A product was calibrated and validated by (Gascon et al., 2017). In this work, the validation of the BOA reflectance product resulting from SEN2COR was based on 24 Aerosol Robotic Network (AERONET) test sites distributed worldwide covering different land cover types and atmospheric conditions. In this case, the validation focused on an area of 9 $km^2$ around each AERONET sun photometer location. The results obtained for different land uses (bare soils, forests and other vegetation covers) were considered consistent and of high-quality, with a divergence on BOA reflectance values of only a 5% (Gascon et al., 2017). It is accepted that field spectroscopy data is the ideal method to ensure

111 an accurate validation of AC methods (McCoy, 2005; Milton et al., 2009), and several studies
112 relied on such measurements (Dörnhöfer et al., 2016; Vuolo et al., 2016). In (Vuolo et al., 2016),
113 two field campaigns with a 350–2500nm range spectroradiometer were performed over an
114 agricultural area in Austria with the objective of validating SEN2COR processor. Although the
115 results obtained were deemed satisfactory, a quantitative measure of the agreement between the
116 two reflectance data sets was not shown in the paper. However, recent studies also reported
117 issues on the performance of these products. In Kukawska et al. (2017) a problem was reported
118 related to the incorrect mask of clouds over artificial structures resulting from SEN2COR
119 processor. According to the authors these errors had a direct influence on the overall accuracy of
120 the classifications performed.

121 Recently, new inter-comparison studies of different AC methods applied to S2 imagery have
122 been published. In Dörnhöfer et al. (2016) the results of three different AC processors were
123 compared with in situ reflectance measurements in an Oligotrophic Lake. The comparison
124 between the in situ reflectance and the reflectance obtained from SEN2COR yielded a root mean
125 square error (RMSE) slightly worse than the other two AC methods. In Lantzanakis et al. (2017)
126 the effectiveness of four AC methods on S2 imagery was compared, three of them physically-
127 based (Second Simulation of a Satellite Signal in the Solar Spectrum (6S), FLAASH and
128 SEN2COR) and one image-based (DOS). The authors concluded that the physically based
129 methods performed better than the image-based one for S2 imagery, but the evaluation was only
130 based on the comparison of BOA reflectances with spectral libraries (Baldridge et al., 2009).
131 Generally, an image-based AC method does not require external data, although the use of the
132 ancillary data required is not currently a drawback due to its increasing availability, easily
133 accessible in an automatic way. In Martins et al. (2017) the assessment of three AC methods, 6SV
134 (6S vector version), ACOLITE and SEN2COR, applied to a S2 image of Amazon Floodplain Lakes,
135 with varying results depending on lake characteristics.

136 At present, one of the most popular algorithms to perform AC on S2 imagery is MAJA
137 (Lonjou et al., 2016), the result of the joint effort of the French Centre National d'Études Spatiales
138 (CNES) and the German Aerospace Center (DLR) to merge their algorithms Multi-Mission
139 Atmospheric Correction and Cloud Screening (MACCS) and ATCOR (Richter and Schläpfer,
140 2015), respectively. MACCS is based on a multi-temporal algorithm that makes an optimized use
141 of image time series to characterize the atmosphere and detect clouds. In (Hagolle et al., 2015b)
142 the AOT retrieval, a key factor in AC, was validated by comparing its value at 0.55 μm to
143 AERONET in situ data. Moreover, BOA reflectances were also validated against in situ
144 measurements (Rouquié et al., 2017) and MODIS BOA reflectance products. Finally, new
145 alternatives to SEN2COR appeared in the last months, such as iCOR (VITO, 2017), implemented
146 as a SNAP plugin to correct S2 and L8 satellite imagery. This processor was previously known as
147 OPERA, and has been tested and validated extensively for MERIS, L8, S2 and PROBA-V in
148 different research projects (ACIX, HIGHROC, INFORM and SPONGE) (Sterckx et al., 2015a). The
149 performance of most of these mentioned processors (MAJA, iCOR, SEN2COR, etc.) have been
150 recently compared in ACIX (Doxani et al., 2018). The comparison was based on BOA reflectances
151 and AOT and WV values and the results varied depending on the sensors, products, and sites.
152 In this context, the aim of this study is to assess the quality of the Level-2A products obtained
153 after the application of four AC processors (SEN2COR, MAJA, 6S and iCOR) using field
154 spectrometry, concretely an Analytical Spectral Device (ASD) FieldSpec® 4. In particular, this
155 work focuses on the accuracy assessment of these products in Mediterranean shrub and
156 grasslands. For that purpose, six permanent plots representative of Mediterranean shrub and
157 grasslands environments and anthropic covers were placed and ground reflectance
158 measurements were acquired simultaneously to four Sentinel-2A overpasses taking into account
159 the requirements to obtain high-quality data. Although, it will be interesting to have in the study
160 area surfaces with reflectances bellow 0.1 or very bright objects in order to assessing better the
161 performance of different atmospheric correction methods, they does not exist in the study area.

Additionally to the S2 spectral bands in the optical spectrum, the accuracy of the Normalized Difference Vegetation Index (NDVI), the Normalized Difference Infrared Index (NDII) and the Normalized Burn Ratio (NBR) derived from them was also evaluated. The performance of cloud detection was not considered in this study due to the lack of ground truth data to compare with.

## 2. Materials and Methods

The methodology was divided into two phases (Fig. 1): (i) The retrieval of input data, consisting of the acquisition of field spectra data and the obtainment of Sentinel-2A data with four different AC and the subsequent calculation of selected spectral indices; and (ii) The validation consisted of a comparative statistical analysis of data obtained from both sources.

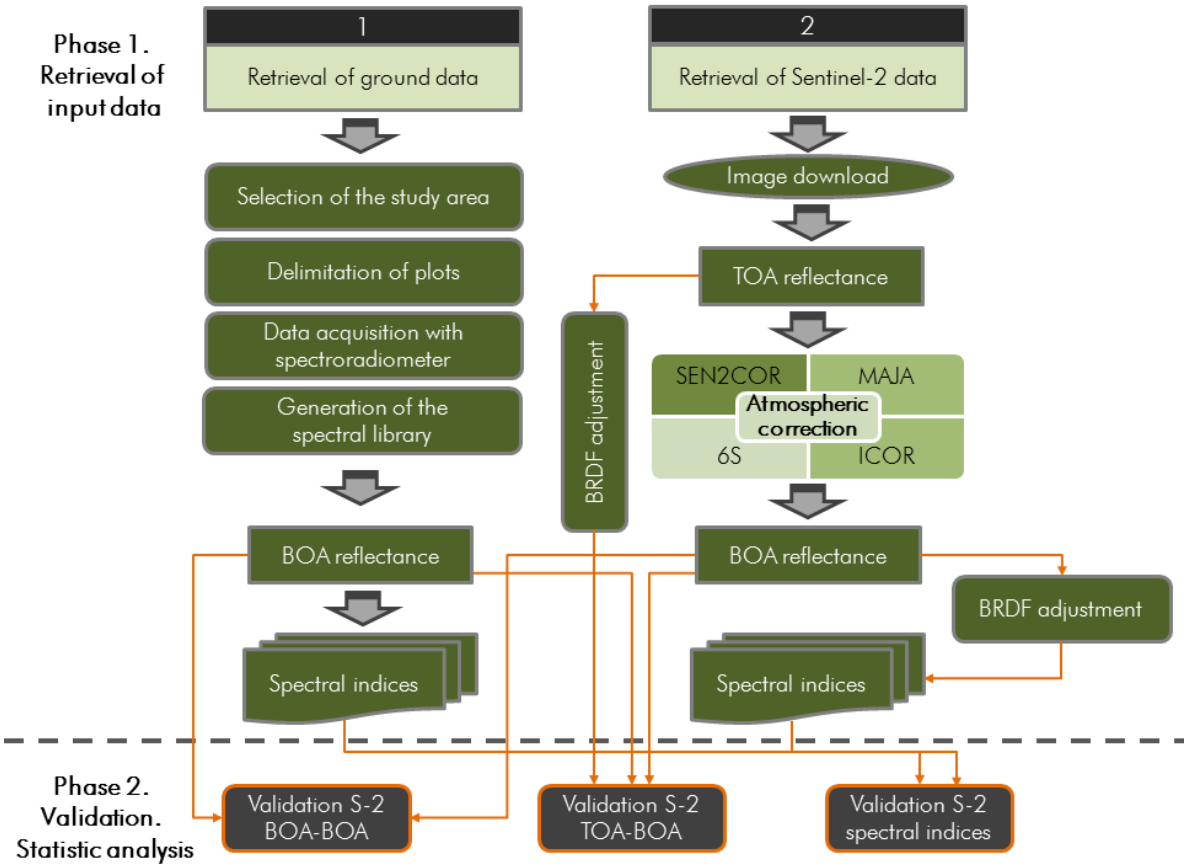


Figure 1. Methodological workflow of the study.

### *2.1. Field spectra data*

174 The selected area to carry out the present study is located in the central sector of the Ebro
175 Basin (Zaragoza, Spain). This area was considered optimal for the purpose of the study due to
176 the presence of stable, homogeneous and extensive typical Mediterranean vegetation, as well as
177 anthropic covers. The plots delimited meet the criteria established by the Committee on Earth
178 Observation Satellites (CEOS) Working group on Calibration and Validation of being placed in
179 sites with low probability of atmospheric variability and having high spatial homogeneity and
180 weak directional effects (Patel et al., 2016), Table 1 contains the description of the six plots
181 delimited, whereas Figure 2 shows their location.

182 **Table 1.** Description of the spectral sampling plots.

| Plot name | Description |
|---|---|
| Asphalt | Asphalt area |
| Grass | Football field |
| Shrub 1 | Main species: *Rosmarinus officinalis L.* |
| Shrub 2 | Main species: *Rosmarinus officinalis L.* |
| Pasture | Main species: *Brachypodium retusum Pers.* |
| Bare soil | Area without vegetation |

183

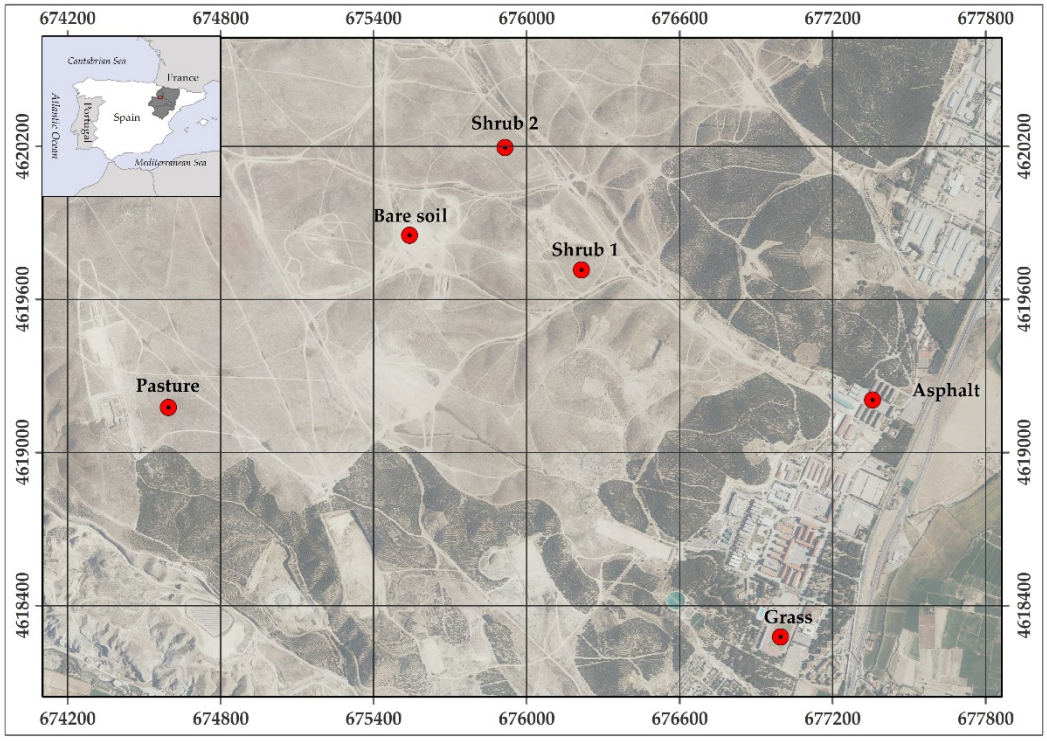


184

185 Figure 2. Location of the spectra sampling plots.

In order to ensure the agreement between the reflectance data obtained by true fieldwork and the S2-derived BOA reflectance values, plots were located according to the following criteria: (i) they were placed on a field path that would allow field spectrometry data acquisition within 2 hours of local solar noon (Milton et al., 2009); (ii) data collection was almost simultaneous to satellite overpasses over the study area (R051 and R094 orbit, between 10:50-11:10 solar time) and in no case exceeded a difference of 2 hours, and (iii) each plot was set at the centroid of the central pixel of a 3 x 3 pixel kernel corresponding to the 20 m grid defined in Sentinel-2A scenes. The 20 m grid of Sentinel-2A scenes was selected because when the field work campaigns were designed, the output of the plugin of Sen2Cor available to SNAP was an image of 10 m or 20 m or 60 m spatial resolution. The imagen of 20 m was chosen, as the majority of the bands MSI have this spatial resolution.

The plots were geo-positioned in field using a Leica VIVA GS15 CS10 real-time kinematic Global Navigation Satellite System, achieving an average planimetric accuracy of 0.50 m. Figure 3 shows the plots staked out in the field. Once the plots were geolocated, the next step was to define two opposing diagonals (NW-SE and NE-SO) with 11 meters length with the aid of a compass and a Vertex (Haglöf Sweden®). These transects marked the itinerary to perform field spectrometry.

203

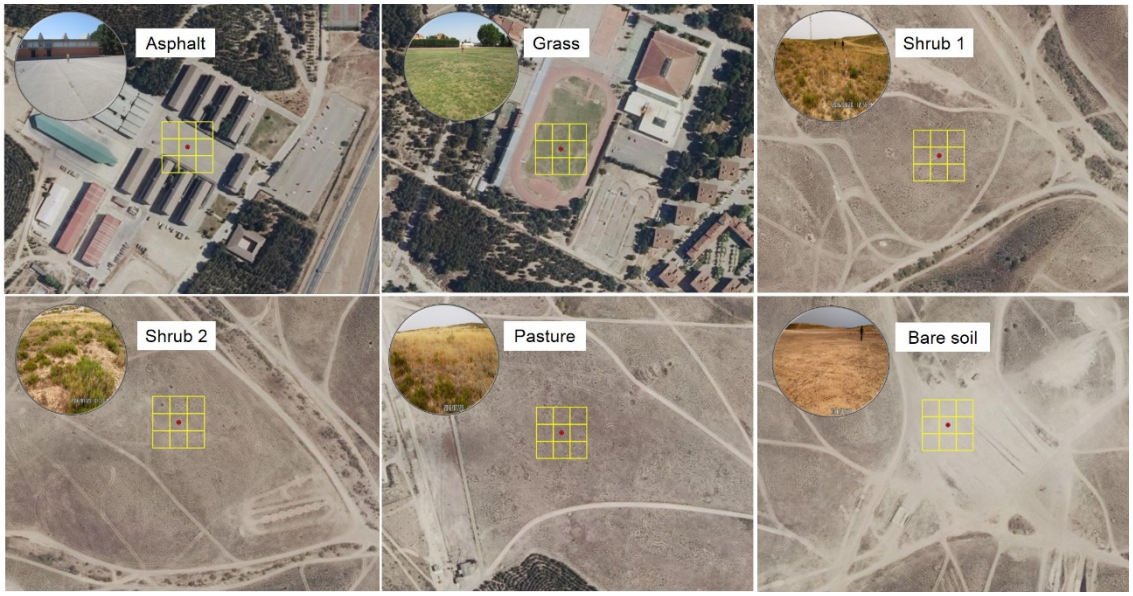


204

205 Figure 3. Plots staked out in field.

206 Measurements of the hemispherical conical reflectance factor (HCRF) (Schaepman-Strub et
207 al., 2006) were captured on clear-sky days using directly an Analytical Spectral Device (ASD)
208 FieldSpec® 4. This instrument has been previously used in vicarious calibration, such as Abdou
209 et al. (2001), Patel et al., (2016); calibration and validation of hyperspectral indices (Le Maire et
210 al., 2008); and for understanding the optical responses of vegetation in field (Pacheco-Labrador
211 et al., 2016). This device is being used in the vicarious calibration campaigns of the hyperespectral
212 sensor EnMAP (Danner, et al., 2015). ASD designed to record the signal throughout the region
213 between the visible (VIS) and near infrared (NIR) (350-1000 nm) and two regions corresponding
214 to the short wave infrared (SWIR) (1001-1800 and 1801-2500 nm) with a sampling interval of 1.4
215 nm – 2 nm, and a spectral resolution Full-Width-Half-Maximum (FWHM) of 3 nm and 10 nm,
216 respectively (ASD, 2015). Following the procedures established in the Spanish National research
217 projects Fluxpec (http://www.lineas.cchs.csic.es/fluxpec/project_overview) and SynerTGE
218 (http://www.lineas.cchs.csic.es/synertge/project_overview) described in Mendiguren el al., 2015;
219 Pacheco-Labrador et al., 2016; Melendo-Vega et al., 2017, before measuring along each transect,

220 dark current was recorded, instrument settings were optimized and reflectance was calibrated
221 using a using a Spectralon® 99% reflective reference panel (Labsphere Inc., North Sutton, NH,
222 USA) l to ensure the perfect correspondence of illumination conditions. With a 1.5 m height and
223 a 25° FOV (Field Of View) (rendering a sensor footprint diameter of about 66 cm), on-the-go
224 measurements of each transect were obtained by averaging 25 individual reflectance spectra for
225 each spectral measurement. Approximately 25 spectral measurements was registered for each
226 transect, resulting 50 per plot. These measurements were used to calculate de average of of each
227 plot every field work date. Table 2 shows the dates of the field work, the number of spectra
228 collected each day and the corresponding Sentinel-2A orbit overpasses. The granules
229 corresponding to the four dates were cloud-free for the study area.
230
231
232

233 **Table 2.** Field work dates,-number of spectra collected and Sentinel-2A orbit overpass.

| Date | No. of spectra | Orbit |
|---|---|---|
| 2016-07-23 | 300 | R094 |
| 2016-08-22 | 315 | R094 |
| 2016-09-01 | 302 | R094 |
| 2016-09-28 | 304 | R051 |

234 *2.2. Calculation of Sentinel-2A bands and spectral indices*

235 A spectral library was generated in ENVI using the field spectra obtained in each sampling
236 day and plot. Every signature was resampled to the spectral response function (SRF) of Sentinel-
237 2A. In this process, signatures following the approach presented in Veraverbeke et al. (2014), the
238 MSI-Sentinel-2A specific noise was added to the simulated MSI using the MSI signal-to-noise
239 ratios (SNR) in 20 m spatial resolution bands (https://earth.esa.int/web/sentinel/user-
240 guides/sentinel-2-msi/resolutions/radiometric) as input to Eq. (1). The objective of this procedure
241 was to ensure that the field spectra were more faithful to the spectral information registered by

MSI sensor. Final signatures were expressed in reflectance given as a fraction of unity. Recently, a new version of the Sentinel-2A SRF has been released by ESA, mainly changing the responses for bands B01 and B02.

$$r_{n,i} = r_i \times \left(1 + \frac{N(0,1)}{SNR_i}\right) \quad (1)$$

where $r_i$ is the reflectance for band i and N(0,1) is a random number generated from a normal distribution with a mean of zero and standard deviation of one.

Finally, the indices NDVI, NDII and NBR were calculated using the Sentinel-2A simulated signatures. These indices were selected due to their popularity in a plethora of applications (i.e., monitoring of vegetation dynamics (Anyamba and Tucker, 2005), estimation of biophysical parameters such as LAI or FCOVER (Carlson and Ripley, 1997) or land degradation assessment (Yengoh et al., 2015) in the case of NDVI, vegetation water content estimation with NDII (Davidson et al., 2006; Yilmaz et al., 2008) or burn severity estimation with NBR (Fraser et al., 2017), their ease of implementation and the fact that they consider spectral bands located on VIS, NIR and SWIR regions.

### *2.3. Obtaining S2 Level-2A product and calculation of spectral indices*

The Level-1C products were acquired simultaneously to field work days (Table 2). Only the T30TXM granule corresponding to the study area was used (100 km²). Subsequently, Level-2A products were generated through four different AC methods at the native resolution of each spectral band. As a result, nine BOA reflectances were obtained for each date and method: three in the visible spectrum (B2, B3 and B4), four in the red edge and NIR (B5, B6, B7 and B8A) and two in the SWIR (B11 and B12).

#### 2.3.1. SEN2COR

SEN2COR (2.4.0 version used, released on August 31 of 2017) is a processor for generating S2 Level-2A products from TOA reflectance Level-1C input data. In short, the following steps are

run through: i) Cloud Detection and Scene Classification, ii) Retrieval of AOT and WV content from the L1C image, and iii) TOA to BOA reflectance conversion. SEN2COR also includes optional cirrus correction, terrain correction and empirical BRDF-corrections. This processor requires a DEM and the LUTs as ancillary data. These LUTs are compiled using an atmospheric RTM based on libRadtran. The LUTs are generated for a wide variety of atmospheric conditions, solar geometries, and ground elevations and are calculated with a spectral resolution of 0.6 nm. This database is subsequently resampled with the S2 spectral responses, in order to obtain the sensor-specific functions needed for the AC. The aerosol optical thickness retrieval is based on the dense dark vegetation (DDV) algorithm. The water vapour retrieval over land is performed with the atmospheric pre-corrected differential absorption (APDA) algorithm. Besides of BOA reflectances, some additional output products are generated, in particular AOT, WV, Scene Classification Maps and Quality Indicators for cloud and snow probabilities. Its output product format is equivalent to the native resolutions of Level-1C imagery, that is, 60, 20 and 10 m. In this work the default parameters were used, neglecting topographic correction, cirrus correction and BRDF correction in order to provide a coherent comparison of AC methods, as the other methods do not include these corrections.

#### 2.3.2. MAJA

The MAJA processor (MACCS ATCOR Joint Algorithm) (Lonjou et al., 2016) is a processor for cloud detection and AC, specifically designed to process time series of optical images at high resolution, acquired under quasi constant viewing angles, such as L8 or S2 images. Since 2016, it is progressively including methods taken from DLR's ATCOR processor. It is now the object of collaboration between CNES, DLR and Centre d'Etudes Spatiales de la BIOsphère (CESBIO). In the first step, MAJA corrects for absorption by atmospheric gas molecules, using the absorption part of the Simplified Model for Atmospheric Correction (SMAC) method and considering ozone, oxygen and water vapor concentrations obtained from either satellite data (ozone, water vapor)

291 or meteorological data (pressure). A second processing step detects the clouds and their shadows,
292 using the multi-temporal cloud detection (MTCD) method. The third step is the AOT estimate,
293 derived from the image, using a combination of three methods: the black pixel method, the dark
294 dense vegetation method (DDV) and the multi-temporal (MT) method. The successive orders of
295 scattering code (SOS) provides LUTs to convert the TOA reflectances already corrected for gas
296 absorption into BOA reflectances. These BOA reflectances are provided with and without
297 topographic correction, at the native spatial resolution of Level-1C products. In this work the
298 latter was selected, with the objective of avoiding confronting factors to the AC. Additionally,
299 MAJA generates a collection of masks including a cloud mask and a geophysical mask.

300 2.3.3. iCOR

301 Implemented as a plugin in SNAP, iCOR (previously known as OPERA) is an AC of S2 and
302 L8 data based on the identification of water and land pixels (VITO, 2017). All input data required
303 by the processor are derived from the image itself or delivered through pre-calculated LUTs. The
304 AC comprises the following steps: i) land and water pixels are identified; ii) AOT is derived from
305 land pixels based on an adapted version of the method developed by Guanter et al. (2007); iii) an
306 adjacency correction is performed using SIMEC (Sterckx et al., 2015b) over water and fixed
307 background ranges over land targets, and iv) the radiative transfer equation is solved. iCOR uses
308 MODTRAN 5 (Berk et al., 2006) LUTs to perform the AC and needs information about the solar
309 and viewing angles and a DEM. Besides of BOA reflectances no additional product is generated.
310 The correction with default parameters has been tested in this work.

311 2.3.4. 6S

312 6S (Second Simulation of the Satellite Signal in the Solar Spectrum) (Vermote et al., 1997) is
313 an open-source AC tool, established itself as one of the standard RTMs used for both remote
314 sensing research and the creation of operational products. In this work AC of S2 imagery was
315 performed with Google Earth Engine (GEE) using Py6S (Murphy, 2017; Wilson, 2013), an

316 interface to the 6S through the Python programming language. The 6S generates interpolated
317 LUTs under different atmospheric conditions, considering altitude of the sensor and target,
318 wavelength and ground reflectance (with the ability to use a number of built-in BRDF models).
319 Essentially, these LUTs are used to calculate AC coefficients which convert TOA radiance to BOA
320 reflectance. In contrast to the previous AC methods, the atmospheric parameters (WV, ozone and
321 AOT) were not obtained from the image itself, but from GEE collections for the place, date and
322 time of acquisition (see Table 3):

323 **Table 3.** Sources of atmospheric parameters obtained in 6S algorithm with GEE.

| Parameter | GEE Collection | Description |
|---|---|---|
| Water vapor | NCEP_RE/surface_wv | Total column water vapor, kg/m² at 6-hour temporal resolution (00:00, 06:00, 12:00, and 18:00 UTC) and 2.5 degree spatial resolution. |
| Ozone | TOMS/MERGED | Total column ozone (Dobson units).The Total Ozone Mapping Spectrometer (TOMS) data represent a merged ozone product from TOMS/EarthProbe, TOMS/Nimbus-7, TOMS/Meteor-3, OMI/Aura and USGS-interpolated data for dates with no data. The resolution ranges from 1.0 x 1.00 deg to 1.0 x 1.25 deg |
| AOT | MODIS/MOD08_M3_051 | MOD08_M3 is a level-3 MODIS gridded atmosphere monthly global product. It contains monthly 1 x 1 degree grid average values of atmospheric parameters. |

324 Level-1C products were downloaded from ESA Open Hub. SEN2COR and ICOR processors
325 used this products as source to generate Level-2A products. Similarly, 6S method was applied to
326 the S2 Level-1C image collection in Google Earth Engine (ID: COPERNICUS/S2). Finally, MAJA
327 level-2A images were downloaded from Theia Land Data Centre.

328 2.3.5. BRDF adjustment

329 The four selected Sentinel 2 images correspond to adjoining paths (orbits R094 and R051).
330 These observations were acquired with directional effects due to surface reflectance anisotropy
331 and changes in the solar and viewing geometry. Therefore, it is required to adjust all images to a
332 uniform nadir view. For that purpose a bidirectional reflectance distribution function (BRDF)
333 correction was applied to TOA and BOA reflectances in order to provide a fair comparison with

334 nadiral ground measurements. The correction was applied following (Roy et al., 2017a; Roy et al.,
335 2017b; Roy et al., 2016) using Google Earth Engine.

336 2.3.6. Calculation of spectral indices.

337 The BOA reflectances of Level-2A products were used as source to calculate three spectral
338 indices: NDVI, one of the most popular index to identify vegetated areas and their condition;
339 NDII, frequently used to estimate soil moisture storage; and NBR, originally designed to identify
340 burned areas and to assess the severity of a burn. In order to calculate these indices from S2 data
341 the following formulation was used:

342 $$NDVI = {(\rho_{B8A} - \rho_{B4})}\Big/{(\rho_{B8A} + \rho_{B4})} \quad (2)$$

343 $$NDII = {(\rho_{B8A} - \rho_{B11})}\Big/{(\rho_{B8A} + \rho_{B11})} \quad (3)$$

344 $$NBR = {(\rho_{B8A} - \rho_{B12})}\Big/{(\rho_{B8A} + \rho_{B12})} \quad (4)$$

345 where, $\rho_{B4}$, $\rho_{B8A}$, $\rho_{B11}$ and $\rho_{B12}$ are BOA reflectances of band B4 (red), band B8A (NIR) and bands
346 B11 and B12 (SWIR) respectively.

347 In the case of NDII and NBR the spatial resolution of both source bands was 20 meters, thus
348 the indices were calculated at this resolution. In contrast, NDVI was calculated at a spatial
349 resolution of 10 meters. Consequently a Nearest Neighbor resampling was applied to downscale
350 band B8A from 20 to 10 meters.

351 *2.4. Statistical analysis for the validation of Level-2A products*

352 The performance of AC methods producing BOA reflectances was evaluated by comparing
353 these reflectances with the ground measurements obtained by the spectroradiometer. This
354 analysis was performed per land cover and band wise in order to obtain more details on the
355 performance of each method. The band 8 is not present in this analysis, as when the first version
356 of the research was performed, this band was not an output at the 20 m spatial resolution obtained

357 from the plugin of Sen2Cor available to SNAP. The evaluation was based on statistical analyses
358 of both datasets, i.e., ground measurement and Sentinel2-derived reflectances. The results of
359 uncorrected Level-1C TOA reflectances were also provided as reference. In particular, the
360 coefficient of determination ($R^2$), and the RMSE were analyzed, besides of spectral signatures of
361 each land cover, and scatterplots of each spectral band. Finally, the three spectral indices
362 mentioned in section 2.3.6. were compared to the results obtained from ground measurements.

363 **3. Results and discussion**

364 The visual assessment of AC shows a clear improvement in visible bands due to the
365 subtraction of atmospheric scattering from the spectral bands with lower wavelength, especially
366 blue band (B2).The RGB composition in true color (blue: B2, green: B3, red: B4) of TOA and BOA
367 reflectances (Level-2A for MAJA algorithm) for each date is shown in Figure 4, with the six plots
368 displayed as red crosses within the study area. The three other methods tested also provided
369 similar visual enhancements.

**(a)** **(b)**

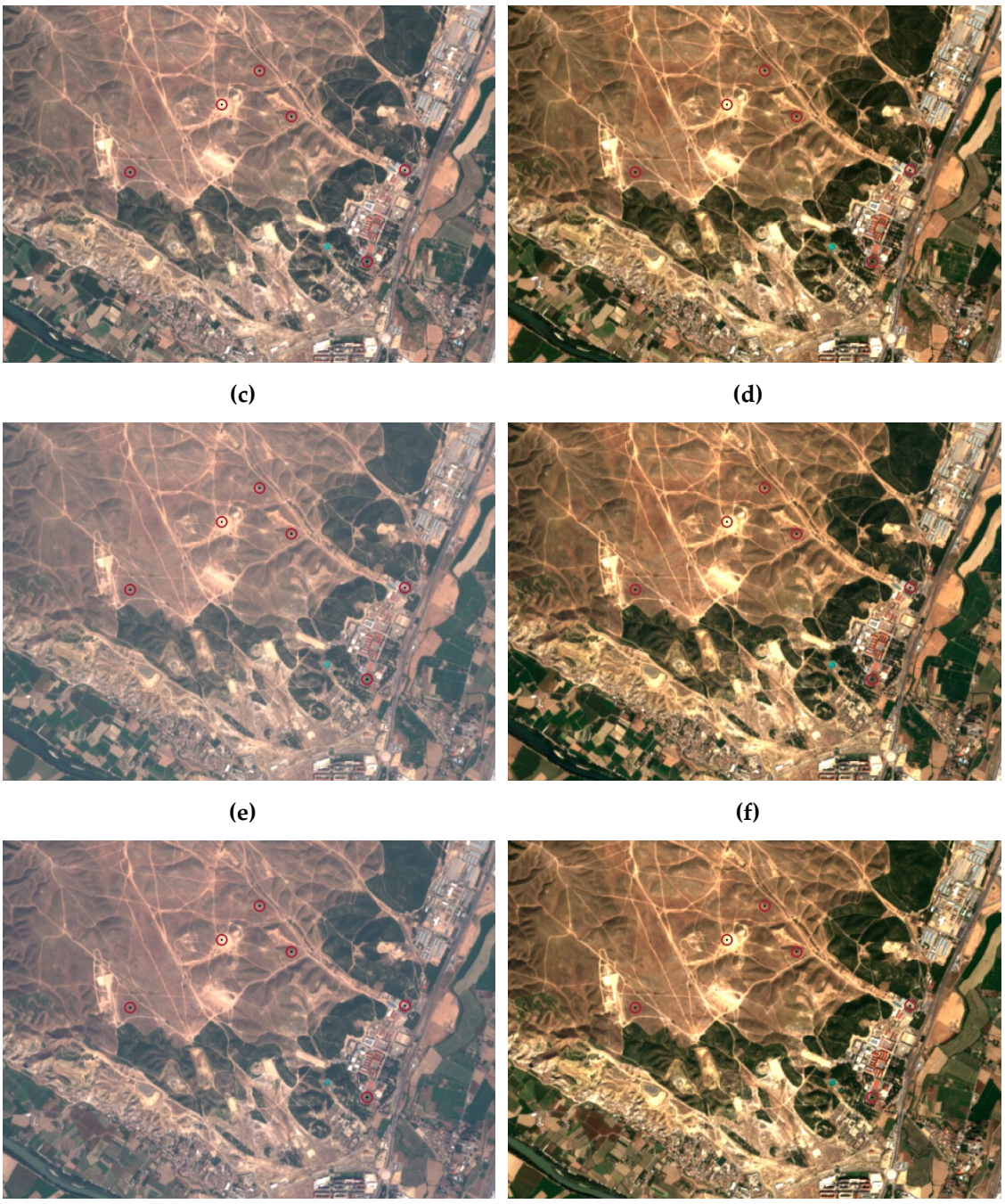


Figure 4. RGB composition of **(a)** TOA reflectance of 23/07 image, **(b)** BOA reflectance (MAJA) of 23/07 image, **(c)** TOA reflectance of 22/08 image, **(d)** BOA reflectance (MAJA) of 22/08 image, **(e)** TOA reflectance of 01/09 image, **(f)** BOA reflectance (MAJA) of 01/09 image, **(g)** TOA reflectance of 28/09 image, **(h)** BOA reflectance (MAJA) of 28/09 image.

### *3.1. Heterogeneity of land covers and radiometric uniformity of the 3 x 3 pixel kernel*

375 As mentioned above, the results of the BRDF-adjusted BOA reflectances generated with each
376 AC method were evaluated both per land cover and per spectral band. Prior to the comparison
377 between ground measured and S2-derived BOA reflectances, a study on the heterogeneity of the
378 field spectra on the different dates was performed, so as to assess the variability per land cover.
379 To this, we used the approximately 200 spectra collected by plot. As illustrated in Table 4, all the
380 plots showed a high homogeneity (i.e., low standard deviation) along the study period, being
381 asphalt the most homogenous cover. This was expected because asphalt is considered to be a
382 pseudo-invariant land cover, composed by a single artificial material and therefore no changes
383 were observed between the four dates.

384 **Table 4.** Standard deviation of the spectra collected in the field along the study season (the
385 spectra collected in the four field dates) per plot and Sentinel 2A band.

| Plot name | B2 | B3 | B4 | B5 | B6 | B7 | B8A | B11 | B12 |
|---|---|---|---|---|---|---|---|---|---|
| Asphalt | 0.003 | 0.003 | 0.003 | 0.004 | 0.008 | 0.007 | 0.007 | 0.004 | 0.005 |
| Pasture | 0.009 | 0.012 | 0.020 | 0.021 | 0.013 | 0.012 | 0.019 | 0.028 | 0.020 |
| Shrub 1 | 0.013 | 0.013 | 0.012 | 0.012 | 0.015 | 0.014 | 0.014 | 0.009 | 0.009 |
| Shrub 2 | 0.002 | 0.004 | 0.005 | 0.006 | 0.008 | 0.008 | 0.012 | 0.012 | 0.011 |
| Grass | 0.009 | 0.012 | 0.018 | 0.019 | 0.020 | 0.021 | 0.023 | 0.020 | 0.013 |
| Bare soil | 0.019 | 0.022 | 0.028 | 0.030 | 0.039 | 0.040 | 0.040 | 0.044 | 0.046 |

386 The category with higher heterogeneity was bare soil. This can be related to the fact that
387 during the study period some off-road driving lessons and exercises were held in the plot,
388 changing the conditions of stoniness and roughness. The rest of the categories (pasture, shrub
389 and grass) showed intermediate values of homogeneity in all the bands. This fact may be due to
390 their rich diversity of species, heterogeneous spatial pattern (presence of different shrubs and
391 grass species and bare soil parches with different degrees of stoniness) and to the drying process
392 of these plant formations throughout the summer. In most cases heterogeneity was higher in NIR
393 and SWIR bands than in visible bands.

394 In order to ensure the radiometric uniformity of the 3 x 3 pixel kernel corresponding to the
395 20 m grid defined in Sentinel-2A scenes for each plot, the coefficient of variation (CV) was

396 calculated using the four L1C scenes together per plot and sensor band. As can be seen in Table
397 5, the CV values obtained are very low, being always lower than 0.05 in all bands, with the only
398 exception of asphalt. As a result, the premise about radiometric uniformity of the 3 x 3 pixel kernel
399 along all the study period is validated, and possible geometric correction errors in Sentinel-2A
400 are avoided. The reason of higher CV values of the asphalt 3x3 kernel is that it includes two pixels
401 that are contaminated by parking roofs spectral response (see Figure 4). This must be in mind in
402 order to read the results obtained to this land cover in the present study.

403 **Table 4.** Coefficient of variation (CV) of the 3 x 3 pixel kernel corresponding to the 20 m grid
404 defined in Sentinel-2A scenes for each plot using the four L1C scenes together per plot and
405 sensor band.

| Plot name | B2 | B3 | B4 | B5 | B6 | B7 | B8A | B11 | B12 |
|---|---|---|---|---|---|---|---|---|---|
| Asphalt | 0.05 | 0.07 | 0.08 | 0.08 | 0.07 | 0.07 | 0.07 | 0.09 | 0.10 |
| Pasture | 0.01 | 0.02 | 0.01 | 0.01 | 0.01 | 0.01 | 0.01 | 0.00 | 0.01 |
| Shrub 1 | 0.01 | 0.01 | 0.01 | 0.03 | 0.03 | 0.03 | 0.03 | 0.02 | 0.02 |
| Shrub 2 | 0.02 | 0.03 | 0.03 | 0,01 | 0,01 | 0,00 | 0.01 | 0.01 | 0.01 |
| Grass | 0,01 | 0,02 | 0,03 | 0,03 | 0,04 | 0.02 | 0.01 | 0,02 | 0,02 |
| Bare soil | 0.04 | 0.03 | 0.03 | 0.02 | 0.02 | 0.02 | 0.02 | 0.01 | 0.02 |

406

407 *3.2. Spectral signatures*

408 The comparison between the field BOA reflectances and S2 images per spectral band and
409 land cover is evaluated in Figure 5, showing the average spectral signature of the four observation
410 dates. In general terms, the highest difference between TOA and BOA reflectances was observed
411 in visible bands, due to the exponential decay of atmospheric scattering effects at longer
412 wavelengths (Martins et al., 2017). The ssphalt plot showed a clear underestimation of TOA
413 reflectance in SWIR bands, which was corrected to a certain degree with AC methods, especially
414 with SEN2COR. On the contrary, minor differences were observed between methods in visible
415 and red edge bands. SEN2COR was the method performing better in the visible bands. In the
416 case of bare soil, higher reflectances were observed in all the spectral bands, as it was expected

417 from this land cover. In the visible bands 6S and MAJA obtained BOA reflectances closer to the
418 ground measurements, whereas iCOR performed better in the red edge and NIR regions. In
419 contrast, 6S showed the best performance in B12 (SWIR). In most of the bands the
420 underestimation of Level-1C TOA reflectance was corrected for this land cover, yet many of the
421 methods tended to over-correct atmospheric effects yielding BOA reflectance values higher than
422 observed field spectral, especially in the NIR.

423 The grass plot showed a typical spectral signature of a vegetated cover, with a clear increase
424 of reflectance from red (B4) to NIR (B8A). Besides, the reduction of reflectance in visible bands
425 after AC was especially clear in this cover with all AC methods that only showed minor
426 differences. On the opposite, red edge and NIR band reflectances were overestimated with the
427 four methods, while SWIR showed better results in all the cases. Finally, in the case of pastures
428 and shrubs (Figures 5d and 5e) the TOA reflectance was clearly overestimated in all the spectral
429 bands and AC methods were not completely successful in correcting these differences. The shrub
430 plot showed better results in the visible bands, were agreement with field spectra improved after
431 AC, especially with MAJA, although in NIR bands the results varied depending on the method.
432 On the contrary, SWIR bands showed a poor performance of Level-2A products, with
433 overestimated reflectances in B11 and B12. In fact, the agreement with the field spectra was worse
434 for the obtained Level-2A products than for the original Level-1C product. Notwithstanding that,
435 the performance of each method could vary if different plots were selected in the comparison.

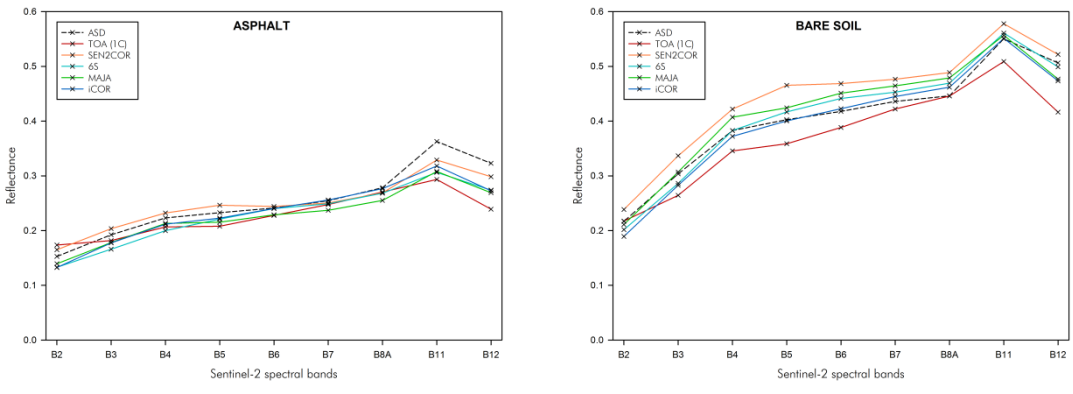


**(a)** **(b)**

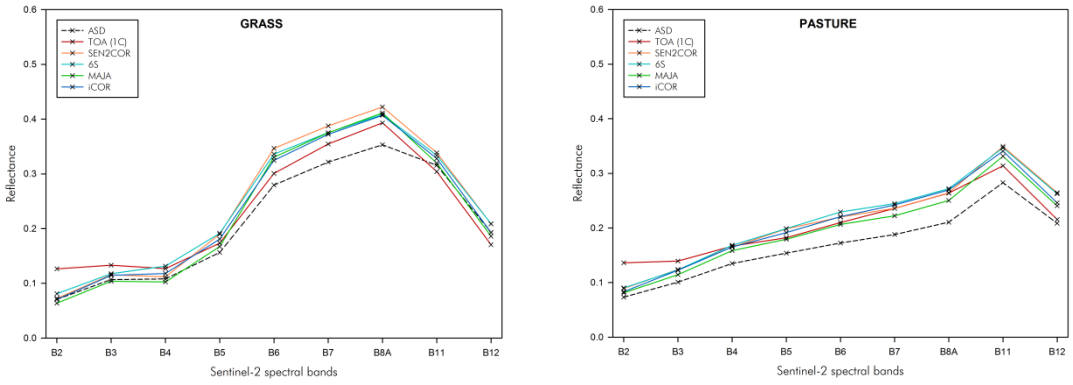


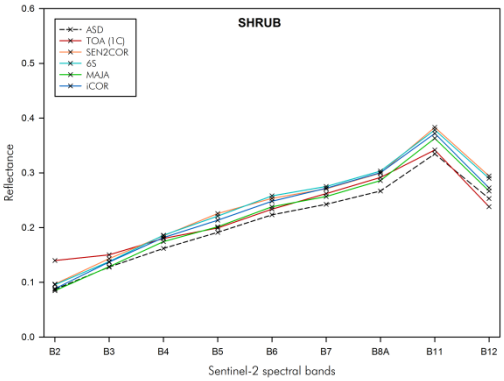


Figure 5. Spectral signatures of five land cover plots for each Level-2A product besides Level-1C uncorrected product. Average of the four dates considered. **(a)** Asphalt plot, **(b)** Bare soil plot, **(c)** Grass plot, **(d)** Pasture and **(e)** Shrub, average of the two shrub plots.

### *3.3. Statistical agreement of the different methods*

The quantitative agreement between field spectra and BOA reflectance values obtained with each AC method was evaluated using $R^2$ and RMSE as figures of merit (Table 5):

**Table 5.** $R^2$ and RMSE obtained per AC method for all the spectral bands and dates. Best method is highlighted in bold.

| | 1C | SEN2COR | 6S | MAJA | iCOR |
|---|---|---|---|---|---|
| **$R^2$** | 0.919 | **0.954** | 0.920 | 0.947 | 0.939 |
| **RMSE** | 0.036 | 0.038 | 0.037 | **0.028** | 0.031 |

The results of Table 5 depict a clear increase in correlation between ground measurements and S2-derived reflectances after AC, with minor differences between methods. Similarly, iCOR

446 and MAJA reduced the RMSE achieved by Level-1C product. However, SEN2COR and 6S only
447 showed slight or no improvement at all.

448 3.3.1. Analysis per land cover

449 Table 6 shows the $R^2$ obtained for each land cover, taking into account the four dates and the
450 nine spectral bands. As it is observed, there is a clear correlation between field spectra and BOA
451 reflectance in all methods, with $R^2$ values equal or higher than 0.90 in all cases, values comparable
452 to those found in another recent study (Lange et al., 2017). Correlations improved clearly after
453 AC correction with higher $R^2$ values achieved by Level-2A products compared to the Level-1C
454 product. Among the land covers, the highest correlation was obtained for grass and shrub, two
455 of the most heterogeneous covers, with the latter showing a great performance with the four AC
456 methods, with minor differences between them. Yet, the degree of improvement after AC (i.e.,
457 comparison between $R^2$ values obtained after and before AC correction), was highest for asphalt.
458 In his case, although differences between methods were stronger (ranging from 0.89 with 6S to
459 0.96 with MAJA), all the methods improved the correlation with the original Level-1C TOA
460 reflectance. Altogether, the comparison between methods does not enable a clear identification
461 of the best method for all cases, although in general ICOR, MAJA and SEN2COR achieved each
462 the highest $R^2$ in two out of five covers.

463

464 **Table 6.** $R^2$ obtained per land cover and AC method. Best method for each cover highlighted in bold

| Land cover | L1C | SEN2COR | 6S | MAJA | iCOR |
|---|---|---|---|---|---|
| ASPHALT | 0.810 | 0.948 | 0.896 | **0.961** | 0.913 |
| BARE SOIL | 0.923 | 0.932 | 0.909 | 0.911 | **0.950** |
| GRASS | 0.936 | **0.974** | 0.962 | 0.970 | **0.974** |
| PASTURE | 0.897 | **0.962** | 0.953 | 0.944 | 0.949 |
| SHRUB | 0.933 | 0.976 | 0.969 | **0.987** | 0.981 |

465 Similarly, Table 7 shows the RMSE obtained per land cover using the four AC methods evaluated.
466 In all the cases the RMSE values were lower than 0.05, with values below 0.02 in the best cases.

467 Generally, the error achieved by Level-1C products decreased after AC, with reductions close to
468 50% of the original error in the best case. The comparison between methods again did not show
469 a clear superior performance of a single method for all the land covers. Asphalt plot shows the
470 lowest RMSE with SEN2COR, while iCOR performed the best with bare soil and grass plots.
471 Finally, MAJA achieved a higher performance with pasture and shrubs. In conclusion, different
472 AC methods showed different results for specific land cover types, in line with Nazeer et al.
473 (2014). Notwithstanding that, further research with a higher number of samples is required to
474 obtain a more complete understanding of the performance of each processor.

475 **Table 7.** RMSE obtained by land cover use. Best method for each cover highlighted in bold

| Land cover | L1C | SEN2COR | 6S | MAJA | iCOR |
|---|---|---|---|---|---|
| ASPHALT | 0.039 | **0.019** | 0.030 | 0.030 | 0.025 |
| BARE SOIL | 0.043 | 0.045 | 0.032 | 0.032 | **0.024** |
| GRASS | **0.033** | 0.043 | 0.040 | 0.034 | **0.033** |
| PASTURE | 0.043 | 0.047 | 0.050 | **0.034** | 0.044 |
| SHRUB | 0.026 | 0.033 | 0.034 | **0.017** | 0.026 |

476 3.3.2. Band wise analysis

477 Table 8 and 9 show the band wise results obtained with the different AC methods. These
478 results were obtained for the four studied dates and for the five land covers. First, $R^2$ values are
479 analyzed (Table 8), suggesting a slight improvement in correlation for all methods if compared
480 to the Level-1C product, with exceptions. Highest correlations were obtained for visible bands
481 (B2, B3 and B4), with $R^2$ values above 0.95 in most cases. Then, $R^2$ values showed a decreasing
482 trend as wavelengths increased, with lower values achieved for Red Edge (B5, B6 and B7), NIR
483 (B8A) and SWIR bands (B11 and B12). The comparison between methods showed minor
484 differences except in the case of the blue band (B2), where $R^2$ ranged from 0.90 in the worst
485 scenario (6S) to 0.97 in the best one (MAJA and iCOR). In contrast, other spectral bands showed
486 very slight differences between methods, and in some bands the highest correlating option was

487 the uncorrected Level-1C product (B6, B7, B8A and B11). The highest correlating method in three
488 out of nine bands was SEN2COR, but differences were minor.

489 **Table 8.** $R^2$ obtained per spectral band. Best method for each band highlighted in bold.

| Spectral band | 1C | SEN2COR | 6S | MAJA | iCOR |
|---|---|---|---|---|---|
| B2 | 0.946 | 0.949 | 0.900 | 0.971 | **0.975** |
| B3 | 0.973 | 0.972 | 0.928 | 0.973 | **0.977** |
| B4 | 0.974 | **0.977** | 0.937 | 0.969 | 0.972 |
| B5 | **0.967** | **0.967** | 0.926 | 0.959 | 0.964 |
| B6 | **0.939** | 0.926 | 0.873 | 0.919 | 0.927 |
| B7 | **0.928** | 0.916 | 0.874 | 0.913 | 0.918 |
| B8A | **0.905** | 0.895 | 0.843 | 0.886 | 0.893 |
| B11 | **0.840** | 0.836 | 0.772 | 0.835 | 0.833 |
| B12 | 0.920 | **0.926** | 0.881 | 0.924 | 0.921 |

490 The comparison of the band wise performance in terms of RMSE showed better results for
491 visible bands, maybe due to the higher spatial resolution, intermediate results for red edge and
492 NIR bands, while SWIR bands showed a poorer performance, with RMSE as high as 0.10 in B12
493 (see Table 9). The RMSE values achieved by the different AC methods showed also minor
494 differences between methods. In some bands, RMSE values after AC were even larger than before
495 AC (bands B6, B7 and B8A). Although differences were not marked, MAJA achieved the lowest
496 overall RMSE with minimum values in bands B2-B5 and also in B11-B12.

497 **Table 9.** RMSE obtained per spectral band. Best method for each band highlighted in bold.

| | 1C | SEN2COR | 6S | MAJA | iCOR |
|---|---|---|---|---|---|
| B2 | 0.047 | 0.018 | 0.019 | **0.010** | 0.016 |
| B3 | 0.029 | 0.023 | 0.022 | **0.012** | 0.017 |
| B4 | 0.026 | 0.027 | 0.028 | **0.020** | 0.021 |
| B5 | 0.026 | 0.042 | 0.034 | **0.020** | 0.025 |
| B6 | **0.025** | 0.045 | 0.044 | 0.033 | 0.033 |
| B7 | **0.029** | 0.043 | 0.042 | 0.034 | 0.037 |
| B8A | **0.033** | 0.046 | 0.046 | 0.038 | 0.041 |
| B11 | 0.039 | 0.047 | 0.047 | **0.038** | 0.040 |
| B12 | 0.099 | 0.104 | 0.101 | **0.076** | 0.083 |

498 *3.4. Scatterplots*

Scatterplots of ground reflectance measurements versus BOA reflectances obtained from S2 Level-2A products (besides of TOA reflectances from Level-1C products as reference) provide help interpreting the values given in tables 5-9. Figure 6 shows the scatterplots of the nine spectral bands considered. In general, Level-1C products overestimated low reflectance values in all spectral bands except B11 and B12. This behavior was especially noticeable in the case of visible bands (B2, B3 and B4), and the performance clearly improved after AC (see Figures 6a, 6b and 6c). On the contrary, a strong underestimation of higher BOA reflectances was observed in all the spectral bands except B8A for the Level-1C product. This effect was higher in SWIR bands (see Figures 6h and 6i), although Level-2A products attenuated this underestimation, especially with SEN2COR and 6S. Again, the comparison between methods did not a show a clear superior method for all the spectral bands and all of them balanced this difference between high and low reflectances. Band B2 (blue) showed a better performance with MAJA with a regression line close to the 1:1 line, while ICOR showed a poor performance due to a clear underestimation of high reflectance values. Bands B3 and B4 followed a similar trend of overestimation of low values and underestimation of high values with Level-1C, which improved after AC, with a superior performance of MAJA. The comparison of methods for red edge ~~spectral~~ bands (see Figures 6d, 6e and 6f) showed a slightly better performance of MAJA, 6S and iCOR methods, in line with the results of Table 9.

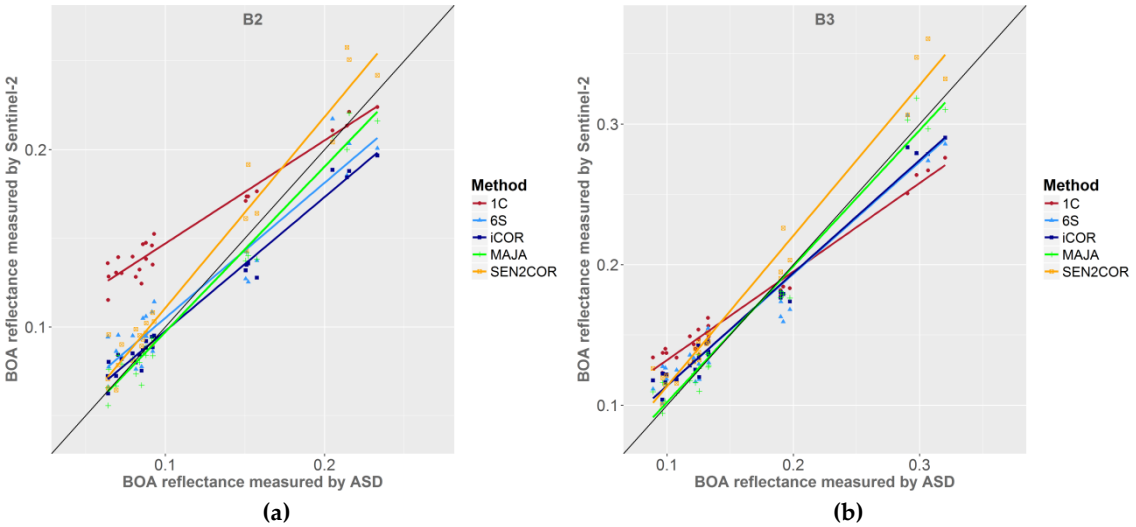


**(a)** **(b)**

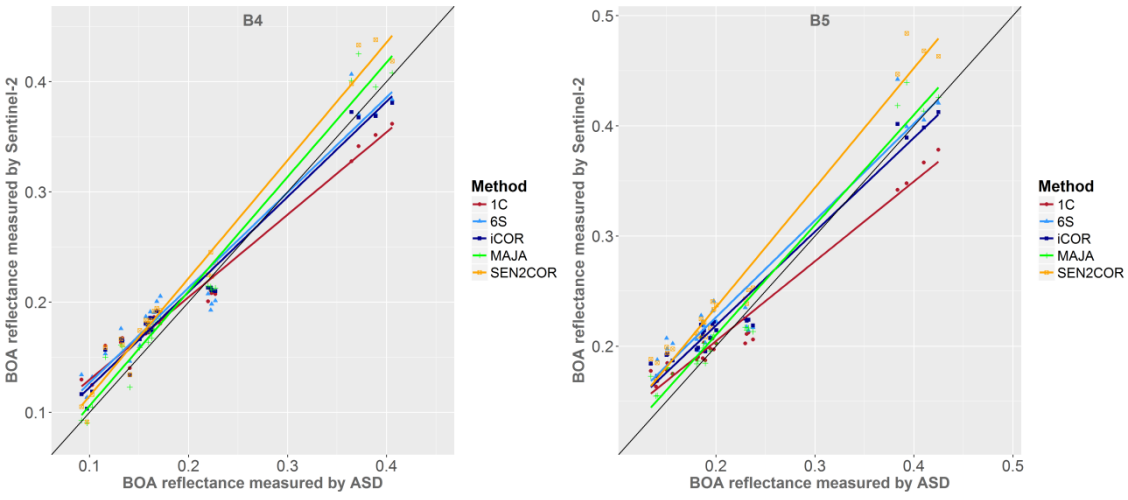
B4
BOA reflectance measured by Sentinel-2
BOA reflectance measured by ASD
Method
1C
6S
iCOR
MAJA
SEN2COR

(c)


B5
BOA reflectance measured by Sentinel-2
BOA reflectance measured by ASD
Method
1C
6S
iCOR
MAJA
SEN2COR

(d)

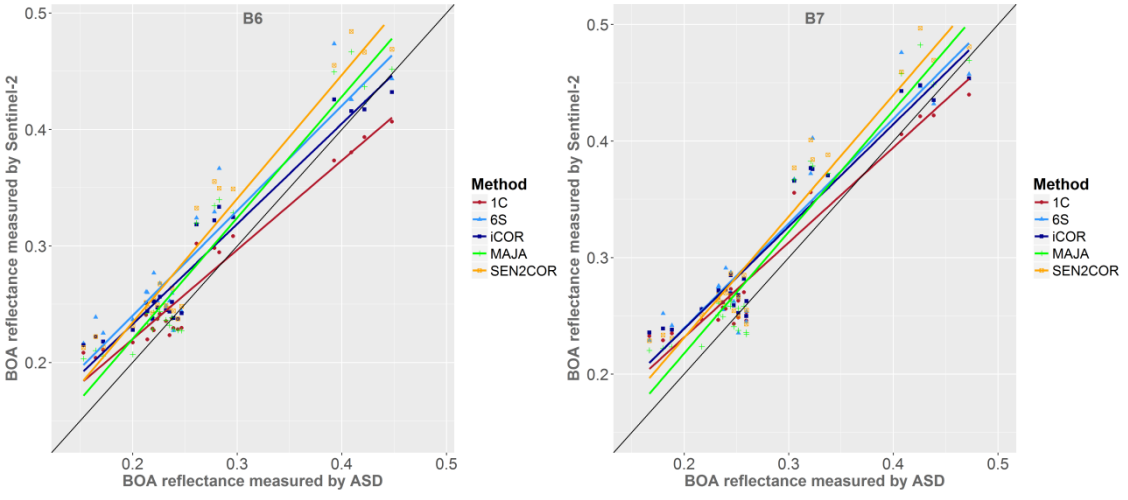
B6
BOA reflectance measured by Sentinel-2
BOA reflectance measured by ASD
Method
1C
6S
iCOR
MAJA
SEN2COR

(e)


B7
BOA reflectance measured by Sentinel-2
BOA reflectance measured by ASD
Method
1C
6S
iCOR
MAJA
SEN2COR

(f)

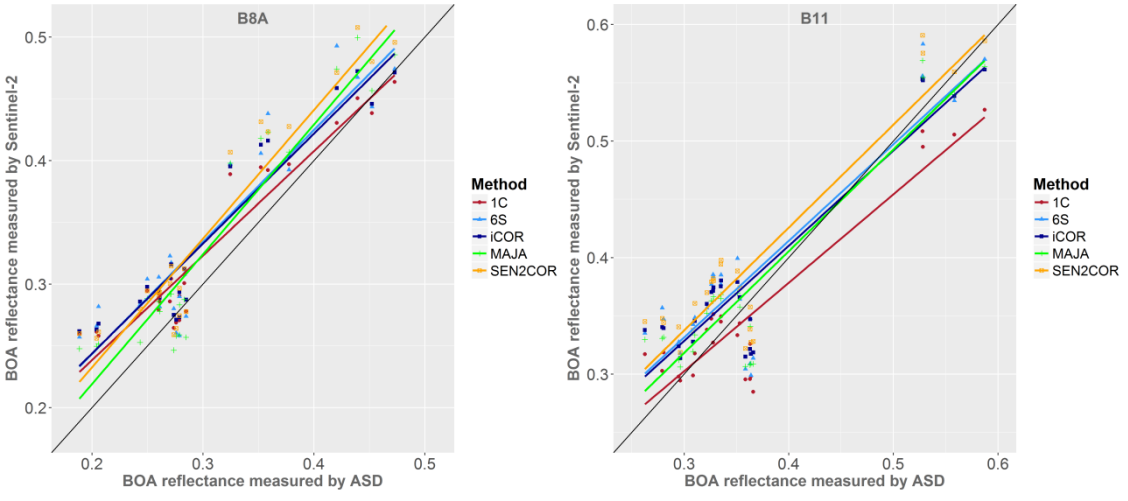
B8A
BOA reflectance measured by Sentinel-2
BOA reflectance measured by ASD
Method
1C
6S
iCOR
MAJA
SEN2COR

(g)


B11
BOA reflectance measured by Sentinel-2
BOA reflectance measured by ASD
Method
1C
6S
iCOR
MAJA
SEN2COR

(h)

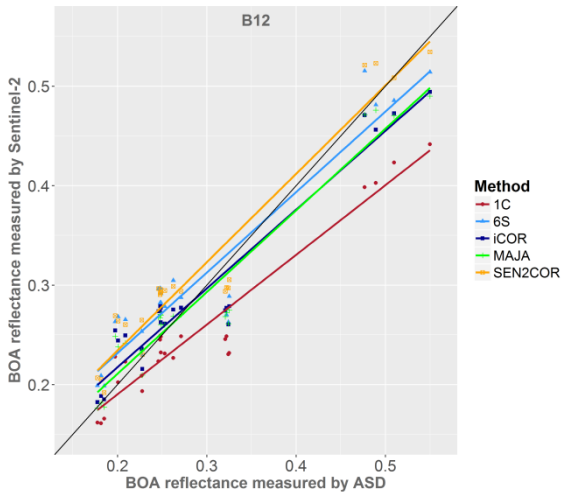


**(i)**

Figure 6. Scatterplot of each spectral band. BOA reflectance measured by ASD in X axis versus BOA reflectance measured by S2 in Y axis.

Finally, the poor performance of Level-1C product at SWIR bands improved clearly after AC. At these bands MAJA showed the best performance at low reflectance values, whereas SEN2COR and 6S achieved the best results at high reflectance values. The underestimation of SWIR BOA reflectances could be due to the results obtained for the asphalt and bare soil plots (see Figure 5a and 5b), where the strong underestimation obtained by Level-1C product, overall in the asphalt plot, was only partially solved by Level-2A products. Possible geometric correction errors in Sentinel 2A scenes could explain this fact, as the spectral response can be partially or totally identified with the roofs includes in two of the 3x3 kernel of this cover.

### *3.5. Assessment of S2-derived spectral indices*

#### 3.5.1. Normalized Difference Vegetation Index (NDVI)

The BOA reflectances of bands B4 and B8A were used as source to calculate NDVI scenes, and subsequently the statistics of the six plots were obtained for the different dates, so as to compare them with the ground measurements. The results of Figure 7a show typical low values of NDVI (lower than 0.3) in pasture, shrub, and specially asphalt and bare soil, consequence of the dry conditions of these dates in the region in the case of vegetated covers, and due to the

typical spectral behavior of man-made surfaces in the case of asphalt. In contrast, grass cover showed a much higher NDVI value, ~0.55 depending the AC method.

Moreover, figure 7b shows the difference in NDVI between the different AC methods and ground measurements-derived NDVI. These results show a slight overestimation of NDVI in most land covers, due to the overestimation of NIR band observed in Figure 5, with the exception of the asphalt cover. These results are in agreement with previous findings, such as Bru et al. (2017), where atmospherically corrected products provided by MACCS (the precursor of MAJA) and 6SV (the vector version of 6S) simulations showed a large overestimation of BOA reflectances, although that work was focused on costal land covers. The comparison of AC methods in Figure 7 shows a better performance of MAJA in every cover except for grass. These results are consistent with Figures 6c and 6g, where this method showed that for high reflectance values band B8A was overestimated. Nevertheless, these higher NDVI values for grass had a direct impact on the quantitative evaluation of this land cover.

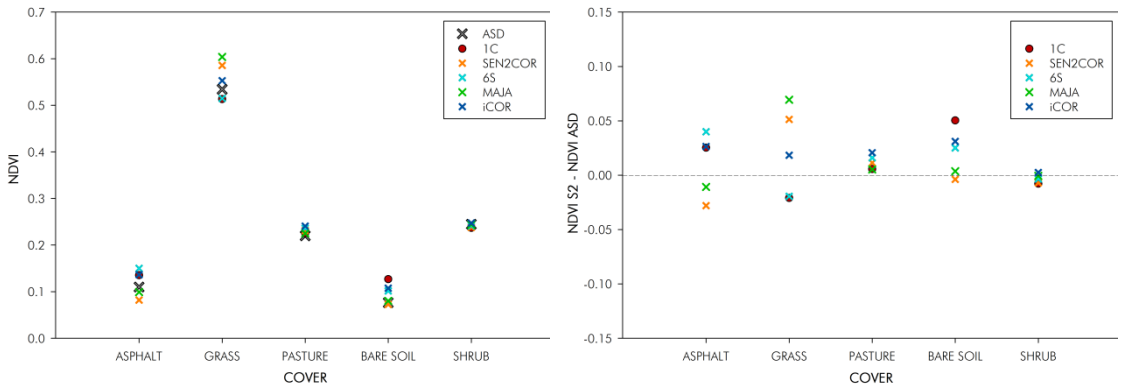


**(a)** **(b)**

Figure 7. **a)** NDVI measured from BOA reflectance of ASD and Sentinel-2 products, **b)** Difference of NDVI measured from ASD and from Sentinel-2 products (NDVI_S2 – NDVI_ASD).

### 3.5.2. Normalized Difference Infrared Index (NDII)

As mentioned above, NDII index is frequently used for estimating vegetation water content. Most vegetated covers in the study period were senescent, so, the negative values achieved by

552 most covers were expected (Fig. 8a) (Yilmaz et al., 2008). On the contrary, values of 0.05 to 0.15
553 were obtained for grass, since it was wetter. Figure 8b shows an overestimation of this index in
554 all covers except for shrubs. The use of AC methods clearly improved the results obtained by
555 Level-1C products, and no clear superior performance of a single method for all the land covers
556 was observed. On the contrary MAJA did not succeed in reducing the overestimation of NDII
557 index of Level-1C product on the grass plot.

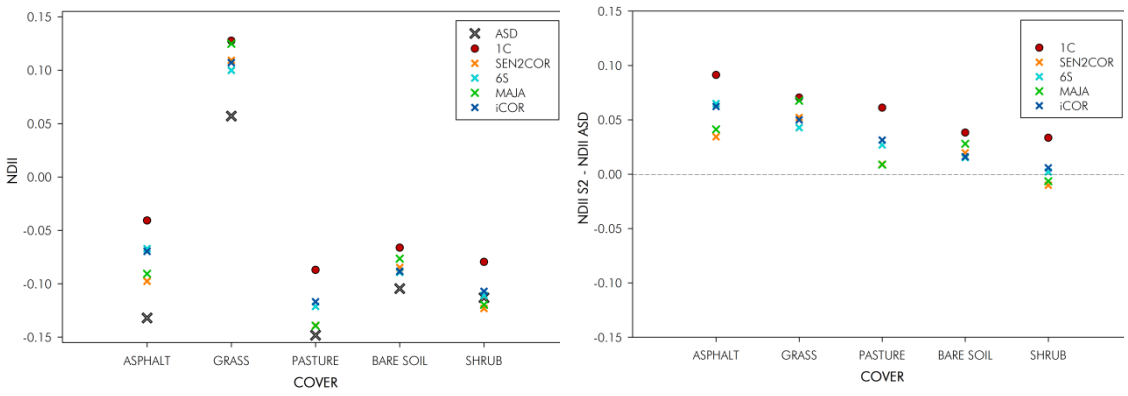


558 Figure 8. **a)** NDII measured from BOA reflectance of ASD and Sentinel-2 products, **b)** Difference of
559 NDII measured from ASD and from Sentinel-2 products (NDII_S2 – NDII_ASD).

560 3.5.3. Normalized Burn Ratio (NBR)

561 In line with the other two spectral indices, NBR (Figure 9a) showed higher values for the
562 grass plot. Additionally, most AC methods showed a clear overestimation on this index too, yet
563 AC improved the fit with ground data in most cases. SEN2COR performed slightly better, with
564 a difference of NBR lower than 0.04 in all land covers. On the contrary, iCOR only partially
565 reduced the overestimation of NBR.

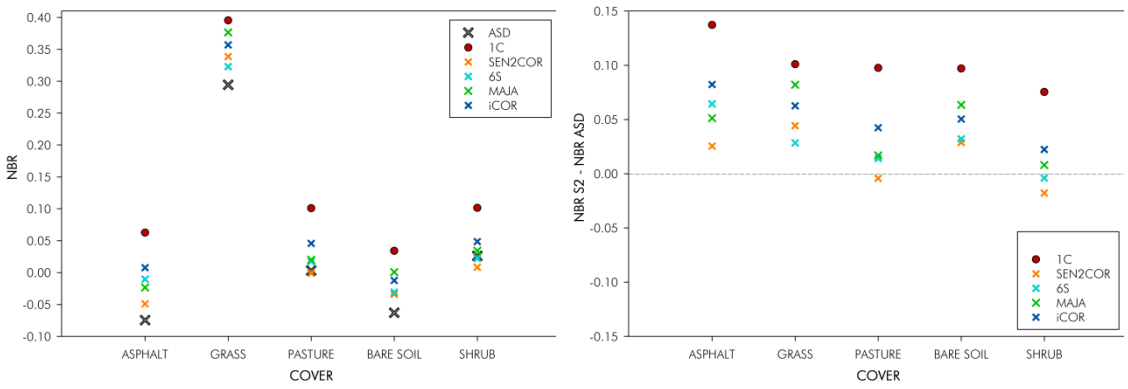


**(a)** **(b)**

Figure 9. **a)** NBR measured from BOA reflectance of ASD and Sentinel-2 products, **b)** Difference of NBR measured from ASD and from Sentinel-2 products (NBR_S2 – NBR_ASD)

### 3.5.4. RMSE of S2- derived spectral indices

Table 10 shows the RMSE between S2-derived spectral indices compared to the ones obtained from ground measurements. Depicted values from Table 10 were consistent with Figures 7, 8 and 9 and agreed with the higher performance of Level-2A-derived spectral indices, compared to the Level-1C product. This improvement was greater in the case of NBR index, probably due to the better performance of BOA reflectances on B12, as seen in Figure 6i. In contrast with the results of Table 5 the lowest RMSE of the different spectral indices were achieved by SEN2COR and iCOR, while MAJA performed slightly worse.

Table 10. RMSE of spectral indices from different AC methods for the six plots and four dates.

Best method for each index highlighted in bold

| RMSE | Level-1C | SEN2COR | 6S | MAJA | iCOR |
|---|---|---|---|---|---|
| NDVI | 0.0316 | 0.0307 | 0.0280 | 0.0307 | **0.0255** |
| NDII | 0.0599 | **0.0304** | 0.0365 | 0.0368 | 0.0370 |
| NBR | 0.1006 | **0.0298** | 0.0350 | 0.0494 | 0.0539 |

Level-1C products showed an overestimation of NDII and NBR indices, which derived in greater RMSE values. These values were clearly reduced by corrected BOA reflectances, in line with the results of Figures 8 and 9. On the contrary, the performance of each AC method in the estimation of NDVI varied for each land cover. This varying performance affected the RMSE

582 values of Table 10, with only minor improvements of RMSE for NDVI index. These results
583 suggest that the selection of the suitable method is application dependent.

584 **4. Conclusions**

585 A rigorous evaluation of the accuracy of Level-2A BOA reflectance products obtained with
586 different AC methods requires their comparison with ground measurements obtained with
587 spectroradiometers. This comparison is necessary to quantify the performance of each AC
588 method both band wise and per land cover. The coefficient of determination or the root mean
589 square error can be used to quantitatively measure this performance, and therefore the different
590 AC methods are evaluated.

591 The results obtained by the RMSE and $R^2$ suggest a varying performance of AC methods
592 depending on the land cover and spectral bands. Although minor differences were observed in
593 most cases, MAJA and iCOR showed a better performance according to the RMSE in the analysis
594 per land cover. Regarding the band wise analysis, MAJA ranked first in all spectral bands. A
595 detailed inspection of the scatterplots, showed a common trend of overestimation of low
596 reflectance values, together with a clear underestimation of high BOA reflectance values in the
597 Level-1C product. This overestimation was more pronounced in band B8A, so the three spectral
598 indices derived from it showed also clear signals of overestimation. Among the AC methods,
599 SEN2COR performed the best in the estimation of two spectral indices (NDII and NBR), while
600 iCOR showed a slightly superior performance in NDVI.

601 Summing up, the results obtained on this inter-comparison of AC methods showed a clear
602 enhancement of the accuracy of BOA reflectance estimation compared to the performance of
603 uncorrected Level-1C product. This proves the need of an accurate AC, essential preprocessing
604 step for a large number of Remote Sensing applications, especially multitemporal studies.
605 Nevertheless, the comparison of four AC methods showed minor differences between them.

606 On the one hand, the statistical analysis of spectral signatures showed a better performance
607 of MAJA, as seen in the figures of merit. On the other hand, the assessment of spectral indices
608 derived from BOA reflectances showed a slightly superior performance of SEN2COR.
609 Consequently, the selection of an AC method needs to be aligned with the study purposes. Yet,
610 this study is based on a reduced amount of comparison points and further research is required to
611 assess the performance of each method on a higher variety of land covers and atmospheric
612 conditions. Besides, the quality of additional products such as geophysical and cloud masks must
613 be assessed to decide which method is the best to correct the S2 imagery.

614 **Acknowledgments:** This work has been supported by the SynerTGE project (CGL2015-69095-R), funded by
615 the Spanish Ministry of Economy and Competitiveness; the HyZCP project (2015-17), funded by the Centro
616 Universitario de la Defensa de Zaragoza, and projects CGL2016-75217-R (MINECO/FEDER, EU) and
617 PyrenEOS EFA 048/15, which has been 65% cofinanced by the European Regional Development through the
618 Interreg V-A Spain-France-Andorra programme (POCTEFA 2014-2020).

619 **Conflicts of Interest:** The authors declare no conflict of interest

620 **References**

621 Abdou, W. A., Conel, J. E., Pilorz, S. H., Helmlinger, M. C., Bruegge, C. J., Gaitley, B. J., Ledeboer,
622 W.C., Martonchik, J. V. 2001. Vicarious calibration a reflectance-based experiment with
623 airMISR. Remote Sensing of Environment 77(3), 338–353.
624 Anyamba, A.; Tucker, C.J. 2005. Analysis of sahelian vegetation dynamics using NOAA-AVHRR
625 NDVI data from 1981–2003. J. Arid Environ. 63, 596-614.
626 ASD inc. 2017. Fieldspec®4 user manual. Boulder (Colorado). Available online:
627 http://support.asdi.com/Products/FileGet.aspx?f=600979-g%20FieldSpec4UG.pdf
628 (Accessed on 1 October 2017).
629 Astrium services. 2013. SPOT 6 & SPOT 7 imagery user guide. Available online:
630 https://www.spaceoffice.nl/blobs/Dataportaal/User_Guide_SPOT6_V1.0.pdf (Accessed
631 on 21 January 2018)
632 Baldridge, A.; Hook, S.; Grove, C.; Rivera, G. 2009. The Aster spectral library version 2.0. Remote
633 Sensing of Environment, 113(4), 711-715.
634 Berk, A., Anderson, G.P., Acharya, P.K., Bernstein, L.S., Muratov, L., Lee, J., Fox, M., Adler-
635 Golden, S.M., Chetwynd, J.H., Hoke, M.L., 2006. MODTRAN5: 2006 update, Algorithms
636 and Technologies for Multispectral, Hyperspectral, and Ultraspectral Imagery XII.
637 International Society for Optics and Photonics, p. 62331F.
638 Borràs, J.; Delegido, J.; Pezzola, A.; Pereira, M.; Morassi, G.; Camps-Valls, G. 2017. Clasificación
639 de usos del suelo a partir de imágenes Sentinel-2, Revista de Teledetección, 48, 55-66.

640 Bru, D., Lubac, B., Normandin, C., Robinet, A., Leconte, M., Hagolle, O., Martiny, N., Jamet, C.,
641 2017. Atmospheric Correction of Multi-Spectral Littoral Images Using a
642 PHOTONS/AERONET-Based Regional Aerosol Model. Remote Sens. 9, 814.
643 Carlson, T.N.; Ripley, D.A. 1997. On the relation between NDVI, fractional vegetation cover, and
644 leaf area index. *Remote Sens. Environ. 62(3), 241-252.*
645 Clevers, J.; Kooistra, L.; van den Brande, M. 2017. Using Sentinel-2 data for retrieving LAI and
646 leaf and canopy chlorophyll content of a potato crop. Remote Sens. 9, 405.
647 Colkesen, I.; Kavzoglu, T. 2017. Ensemble-based canonical correlation forest (CCF) for land use
648 and land cover classification using Sentinel-2 and Landsat OLI imagery. Remote Sens.
649 Lett. 8, 1082-1091.
650 Chrysafis, I.; Mallinis, G.; Siachalou, S.; Patias, P. 2017. Assessing the relationships between
651 growing stock volume and Sentinel-2 imagery in a mediterranean forest ecosystem.
652 Remote Sens. Lett. 8, 508-517.
653 Chuvieco, E. 2010. Teledetección espacial: La observación de la tierra desde el espacio. Madrid.
654 ISBN: 978-84-344-3498-1.
655 Danner, M.; Locherer, M.; Hank, T.; Richter, K. 2015. Spectral Sampling with the ASD FieldSpec
656 4 – Theory, Measurement, Problems, Interpretation. EnMAP Field Guides Technical
657 Report, GFZ Data Services. http://doi.org/10.2312/enmap.2015.008.
658 Davidson, A.; Wang, S.; Wilmshurst, J. 2006. Remote sensing of grassland–shrubland vegetation
659 water content in the shortwave domain. Int. J. Appl. Earth Obs. Geoinf. 8, 225-236.
660 Doxani, G., Vermote, E., Roger, J.-C., Gascon, F., Adriaensen, S., Frantz, D., Hagolle, O., Hollstein,
661 A., Kirches, G., Li, F., Louis, J., Mangin, A., Pahlevan, N., Pflug, B., Vanhellemont, Q.,
662 2018. Atmospheric Correction Inter-Comparison Exercise. Remote Sens. 10, 352.
663 Dörnhöfer, K.; Göritz, A.; Gege, P.; Pflug, B.; Oppelt, N. 2016. Water constituents and water depth
664 retrieval from Sentinel-2A—A first evaluation in an oligotrophic lake. Remote Sens. 8,
665 941.
666 Drusch, M.; Del Bello, U.; Carlier, S.; Colin, O.; Fernandez, V.; Gascon, F.; Hoersch, B.; Isola, C.;
667 Laberinti, P.; Martimort, P., et al., 2012. Sentinel-2: ESA's Optical High-Resolution
668 Mission for GMES operational services. Remote Sens. Environ. 120, 25-36.
669 ESA, 2015. Sentinel-2 User Handbook, in: Agency, E.S. (Ed.).
670 Fraser, R.; van der Sluijs, J.; Hall, R. 2017. Calibrating satellite-based indices of burn severity from
671 UAV-derived metrics of a burned boreal forest in NWT, Canada. Remote Sens. 9, 279.
672 Gascon, F.; Bouzinac, C.; Thépaut, O.; Jung, M.; Francesconi, B.; Louis, J.; Lonjou, V.; Lafrance, B.;
673 Massera, S.; Gaudel-Vacaresse, A., et al. 2017. Copernicus Sentinel-2A calibration and
674 products validation status. Remote Sens. 9, 584.
675 Guanter Palomar, L., 2007. New algorithms for atmospheric correction and retrieval of
676 biophysical parameters in Earth Observation. Application to ENVISAT/MERIS data.
677 Universitat de València.
678 Hagolle, O., Huc, M., Villa Pascual, D., Dedieu, G., 2015a. A Multi-Temporal and Multi-Spectral
679 Method to Estimate Aerosol Optical Thickness over Land, for the Atmospheric
680 Correction of FormoSat-2, LandSat, VENμS and Sentinel-2 Images. Remote Sens. 7, 2668.
681 Hagolle, O.; Sylvander, S.; Huc, M.; Claverie, M.; Clesse, D.; Dechoz, C.; Lonjou, V.; Poulain, V.
682 2015b. Spot-4 (take 5): Simulation of Sentinel-2 time series on 45 large sites. Remote Sens.,
683 7, 12242.
684 Immitzer, M.; Vuolo, F.; Atzberger, C. 2016. First experience with Sentinel-2 data for crop and
685 tree species classifications in central Europe. Remote Sens. 8, 166.
686 Korhonen, L.; Hadi; Packalen, P.; Rautiainen, M. 2017. Comparison of Sentinel-2 and Landsat 8
687 in the estimation of boreal forest canopy cover and leaf area index. Remote Sens. Environ.
688 195, 259-274.

689 Kukawska, E.; Lewinski, S.; Krupinski, M.; Malinowski, R.; Nowakowski, A.; Rybicki, M.;
690 Kotarba, A. 2017. Multitemporal Sentinel-2 data - remarks and observations. In 9th
691 International Workshop on the Analysis of Multitemporal Remote Sensing Images.
692 Lange, M., Dechant, B., Rebmann, C., Vohland, M., Cuntz, M., Doktor, D., 2017. Validating
693 MODIS and Sentinel-2 NDVI products at a temperate deciduous forest site using two
694 independent ground-based sensors. Sensors, 17, 1855.
695 Lantzanakis, G.; Mitraka, Z.; Chrysoulakis, N. 2017. Comparison of physically and image based
696 atmospheric correction methods for Sentinel-2 satellite imagery. In Perspectives on
697 atmospheric sciences, Springer, 255-261.
698 Le Maire, G., François, C., Soudani, K., Berveiller, D., Pontailler, J. Y., Bréda, N., Genet, H., Davi,
699 H., Dufrêne, E. 2008. Calibration and validation of hyperspectral indices for the
700 estimation of broadleaved forest leaf chlorophyll content, leaf mass per area, leaf area
701 index and leaf canopy biomass. Remote Sensing of Environment, 112(10), 3846–3864.
702 Lebourgeois, V.; Dupuy, S.; Vintrou, É.; Ameline, M.; Butler, S.; Bégué, A. 2017. A combined
703 random forest and OBIA classification scheme for mapping smallholder agriculture at
704 different nomenclature levels using multisource data (simulated Sentinel-2 time series,
705 VHRS and DEM). Remote Sens. 9, 259.
706 Louis, J., Debaecker, V., Pflug, B., Main-Knorn, M., Bieniarz, J., Mueller-Wilm, U., Cadau, E.,
707 Gascon, F., 2016. Sentinel-2 Sen2Cor: L2A Processor for Users, Proceedings Living Planet
708 Symposium 2016. Spacebooks Online, pp. 1-8.
709 Lefebvre, A.; Sannier, C.; Corpetti, T. 2016. Monitoring urban areas with Sentinel-2A data:
710 Application to the update of the Copernicus high resolution layer imperviousness
711 degree. Remote Sens. 8, 606.
712 Lillesand, T.; Kiefer, R.W.; Chipman, J. 2014. Remote sensing and image interpretation. John
713 Wiley & Sons. ISBN: 978-1118343289
714 Lonjou, V.; Desjardins, C.; Hagolle, O.; Petrucci, B.; Tremas, T.; Dejus, M.; Makarau, A.; Auer, S.
715 2016. MACCS-ATCOR joint algorithm (MAJA), In Proceedings of SPIE - The
716 International Society for Optical Engineering.
717 Mallinis, G.; Mitsopoulos, I.; Chrysafi, I. 2017. Evaluating and comparing Sentinel 2A and
718 Landsat-8 Operational Land Imager (OLI) spectral indices for estimating fire severity in
719 a Mediterranean pine ecosystem of Greece. GIScience & Remote Sens. 55, 1-18.
720 McCoy, R.M. 2005. Field spectroscopy. In Field methods in remote sensing, Guilford Press, New
721 York, 42-58. ISBN: 978-1593850791
722 Marcello, J.; Eugenio, F.; Perdomo, U.; Medina, A. 2016. Assessment of atmospheric algorithms
723 to retrieve vegetation in natural protected areas using multispectral high resolution
724 imagery. Sensors, 16, 1624.
725 Martins, V.S.; Barbosa, C.C.F.; de Carvalho, L.A.S.; Jorge, D.S.F.; Lobo, F.L.; de Moraes Novo,
726 E.M.L. 2017. Assessment of atmospheric correction methods for Sentinel-2 MSI images
727 applied to amazon floodplain lakes. Remote Sens. 9, 322.
728 Melendo-Vega, J.R., Martín, M.P., Vilar del Hoyo, L., Pacheco-Labrador, J., Echavarría, P.,
729 Martínez-Vega, J. 2017. Estimation of grassland biophysical parameters in a "dehesa"
730 ecosystem from field spectroscopy and airborne hyperspectral imagery. Revista de
731 Teledetección 48, 13-28.
732 Mendiguren, G., Martín, P. Nieto, H., Pacheco-Labrador, J., Jurdao, S. 2015. Seasonal variation in
733 grass water content estimated from proximal sensing and MODIS time series in a
734 Mediterranean Fluxnet site. Biogeosciences 12 (18), 5523-5535.
735 Milton, E.J.; Schaepman, M.E.; Anderson, K.; Kneubühler, M.; Fox, N. 2009. Progress in field
736 spectroscopy. Remote Sens. Environ. 113, S92-S109.
737 Müller-Wilm, U. 2017. Sentinel-2 MSI – Level-2A prototype processor installation and user
738 manual. Available online: http://step.esa.int/thirdparties/sen2cor/2.2.1/S2PAD-VEGA-
739 SUM-0001-2.2.pdf (Accessed on 28 November 2017).

740 Munyati, C. 2017. The potential for integrating Sentinel 2 MSI with Spot 5 HRG and Landsat 8
741 OLI imagery for monitoring semi-arid savannah woody cover. Int. J. Remote Sens. 38,
742 4888-4913.
743 Murphy, S. 2017. Github repository of Sam Murphy. Available online:
744 https://github.com/samsammurphy (Accessed on 1 of December 2017).
745 Navarro, G.; Caballero, I.; Silva, G.; Parra, P.-C.; Vázquez, Á.; Caldeira, R. 2017. Evaluation of
746 forest fire on Madeira island using Sentinel-2A MSI imagery. Int. J. Appl. Earth Obs.
747 Geoinf. 58, 97-106.
748 Nazeer, M., Nichol, J.E., Yung, Y.-K., 2014. Evaluation of atmospheric correction models and
749 Landsat surface reflectance product in an urban coastal environment. Int J Remote Sens
750 35, 6271-6291.
751 Novelli, A.; Aguilar, M.A.; Nemmaoui, A.; Aguilar, F.J.; Tarantino, E. 2016. Performance
752 evaluation of object based greenhouse detection from Sentinel-2 MSI and Landsat 8 OLI
753 data: A case study from Almería (Spain). Int. J. Appl. Earth Obs. Geoinf. 52, 403-411.
754 Paul, F.; Winsvold, S.; Kääb, A.; Nagler, T.; Schwaizer, G. 2016. Glacier remote sensing using
755 Sentinel-2. Part II: Mapping glacier extents and surface facies, and comparison to Landsat
756 8. Remote Sens. 8, 575.
757 Pacheco-Labrador, J., Martín, M. P., Riaño, D., Hilker, T., Carrara, A. 2016. New approaches in
758 multi-angular proximal sensing of vegetation: Accounting for spatial heterogeneity and
759 diffuse radiation in directional reflectance distribution models. Remote Sensing of
760 Environment 187, 447–457.
761 Patel, P. N., Bhatt, H., Mathur, A. K., Prajapati, R. P., Tyagi, G. 2016. Reflectance-based vicarious
762 calibration of INSAT-3D using high-reflectance ground target. Remote Sensing
763 Applications: Society and Environment 3, 20–35.
764 Pesaresi, M.; Corbane, C.; Julea, A.; Florczyk, A.; Syrris, V.; Soille, P. 2016. Assessment of the
765 added-value of Sentinel-2 for detecting built-up areas. Remote Sens. 8, 299.
766 Pons, X.; Pesquer, L.; Cristóbal, J.; González-Guerrero, O. 2014. Automatic and improved
767 radiometric correction of Landsat imagery using reference values from MODIS surface
768 reflectance images. Int. J. Appl. Earth Obs. Geoinf. 33, 243-254.
769 Quintano, C.; Fernández-Manso, A.; Fernández-Manso, O. 2016. Sentinel-2A red-edge spectral
770 indices suitability for discriminating burn severity. Int. J. Appl. Earth Obs. Geoinf. 50,
771 170-175.
772 Richter, R.; Louis, J.; Berthelot, B. 2017. Sentinel-2 MSI – Level 2A products algorithm theoretical
773 basis document. Available online: https://earth.esa.int/c/document_library/
774 get_file?folderId=349490&name=DLFE-4518.pdf (Accessed on 28 November 2017).
775 Richter, R.; Schläpfer, D. 2015. ATCOR-2/3 user guide, version 9.0.0. DLR report DLR-IB, 565-01.
776 Rouquié, B., Hagolle, O., Bréon, F.-M., Boucher, O., Desjardins, C., Rémy, S., 2017. Using
777 Copernicus Atmosphere Monitoring Service Products to Constrain the Aerosol Type in
778 the Atmospheric Correction Processor MAJA. Remote Sens. 9, 1230.
779 Roy, D., Li, Z., Zhang, H., 2017a. Adjustment of Sentinel-2 Multi-Spectral Instrument (MSI) Red-
780 Edge Band Reflectance to Nadir BRDF Adjusted Reflectance (NBAR) and Quantification
781 of Red-Edge Band BRDF Effects. Remote Sensing 9, 1325.
782 Roy, D.P., Li, J., Zhang, H.K., Yan, L., Huang, H., Li, Z., 2017b. Examination of Sentinel-2A multi-
783 spectral instrument (MSI) reflectance anisotropy and the suitability of a general method
784 to normalize MSI reflectance to nadir BRDF adjusted reflectance. a School of Surveying,
785 University of Otago. PO Box 56, Dunedin, New Zealand 199, 25-38.
786 Roy, D.P., Zhang, H.K., Ju, J., Gomez-Dans, J.L., Lewis, P.E., Schaaf, C.B., Sun, Q., Li, J., Huang,
787 H., Kovalskyy, V., 2016. A general method to normalize Landsat reflectance data to nadir
788 BRDF adjusted reflectance. a School of Surveying, University of Otago. PO Box 56,
789 Dunedin, New Zealand 176, 255-271.

790 Schaepman-Strub, G.; Schaepman, M.E.; Painter, T.H.; Dangel, S.; Martonchik, J.V. 2006.
791 Reflectance quantities in optical remote sensing—definitions and case studies. Remote
792 Sens. Environ. 103(1), 27-42.
793 Shoko, C.; Mutanga, O. 2017, Examining the strength of the newly-launched Sentinel 2 MSI sensor
794 in detecting and discriminating subtle differences between C3 and C4 grass species.
795 ISPRS J. Photogramm. Remote Sens. 129, 32-40.
796 Sibanda, M.; Mutanga, O.; Rouget, M. 2016. Comparing the spectral settings of the new
797 generation broad and narrow band sensors in estimating biomass of native grasses
798 grown under different management practices. GIScience & Remote Sens, 53, 614-633.
799 Sterckx, S., Knaeps, E., Adriaensen, S., Reusen, I., De Keukelaere, L., Hunter, P., Giardino, C.,
800 Odermatt, D., 2015a. OPERA: An atmospheric correction for land and water, Proceedings
801 of the ESA Sentinel-3 for Science Workshop, Venice, Italy, pp. 2-5.
802 Sterckx, S., Knaeps, S., Kratzer, S., Ruddick, K., 2015b. SIMilarity Environment Correction
803 (SIMEC) applied to MERIS data over inland and coastal waters. Remote Sens Environ
804 157, 96-110.
805 Toming, K.; Kutser, T.; Laas, A.; Sepp, M.; Paavel, B.; Nõges, T. 2016. First experiences in mapping
806 lake water quality parameters with Sentinel-2 MSI imagery. Remote Sens. 8, 640.
807 Traganos, D.; Reinartz, P. 2017. Mapping Mediterranean seagrasses with Sentinel-2 imagery.
808 Marine Pollution Bulletin.
809 Van der Meer, F.D., van der Werff, H.M.A., van Ruitenbeek, F.J.A., 2014. Potential of ESA's
810 Sentinel-2 for geological applications. Remote Sens. Environ. 148, 124–133.
811 Verhegghen, A.; Eva, H.; Ceccherini, G.; Achard, F.; Gond, V.; Gourlet-Fleury, S.; Cerutti, P. 2016.
812 The potential of Sentinel satellites for burnt area mapping and monitoring in the Congo
813 basin forests. Remote Sens. 8, 986.
814 Veraverbeke, S.; Stavros, E.N.; Hook, S.J. 2014. Assessing fire severity using imaging spectroscopy
815 data from the Airborne Visible/Infrared Imaging Spectrometer (AVIRIS) and comparison
816 with multispectral capabilities. Remote Sens. Environ. 154, 153-163.
817 Vermote, E.F., Kotchenova, S., 2008. Atmospheric correction for the monitoring of land surfaces.
818 Journal of Geophysical Research: Atmospheres 113.
819 Vermote, E.F., Tanré, D., Deuze, J.L., Herman, M., Morcette, J.-J., 1997. Second simulation of the
820 satellite signal in the solar spectrum, 6S: An overview. IEEE Trans. Geosci. Remote Sens.
821 35, 675-686.
822 VITO Remote Sensing. 2017. Available online: https://blog.vito.be/remotesensing/ icor_available
823 (Accessed on 27 November 2017).
824 Vuolo, F.; Żółtak, M.; Pipitone, C.; Zappa, L.; Wenng, H.; Immitzer, M.; Weiss, M.; Baret, F.;
825 Atzberger, C. 2016. Data service platform for Sentinel-2 surface reflectance and value-
826 added products: System use and examples. Remote Sens. 8, 938.
827 Wilson, R.T., 2013. Py6S: A Python interface to the 6S radiative transfer model. Computers and
828 Geosciences 51, 166-171.
829 Yang, X.; Chen, L. 2017. Evaluation of automated urban surface water extraction from Sentinel-
830 2A imagery using different water indices. J. Appl. Remote Sens. 11, 026016
831 Yengoh, G.T.; Dent, D.; Olsson, L.; Tengberg, A.E.; Tucker III, C.J. 2015. Use of the normalized
832 difference vegetation index (NDVI) to assess land degradation at multiple scales: Current
833 status, future trends, and practical considerations. Springer. ISBN: 978-3-319-24112-8.
834 Yilmaz, M.T.; Hunt, E.R.; Jackson, T.J. 2008. Remote sensing of vegetation water content from
835 equivalent water thickness using satellite imagery. Remote Sens. Environ. 112, 2514-2522.
836 Zanter, K. 2015. Landsat 8 (L8) data users handbook. Department of the Interior US Geological
837 Survey.